CrossMark

Electromagnetic Signatures of Relativistic Explosions in the Disks of Active Galactic Nuclei

Rosalba Perna[1,2] , Davide Lazzati[3] , and Matteo Cantiello[2,4]

[1] Department of Physics and Astronomy, Stony Brook University, Stony Brook, NY 11794-3800, USA
[2] Center for Computational Astrophysics, Flatiron Institute, New York, NY 10010, USA
[3] Department of Physics, Oregon State University, 301 Weniger Hall, Corvallis, OR 97331, USA
[4] Department of Astrophysical Sciences, Princeton University, Princeton, NJ 08544, USA

Abstract

The disks of active galactic nuclei (AGNs), traditionally studied as feeders of the supermassive black holes (SMBHs) at their centers, are also hosts to massive stars and hence their neutron star (NS) and black hole (BH) remnants. Migration traps and gas torques in these disks favor binary formation and enhance the rate of compact object mergers. In these environments both long gamma-ray bursts (GRBs) from the death of massive stars and short GRBs from NS–NS to NS–BH mergers are expected. However, their properties in the environment of AGN disks have never been studied. Here we show that GRBs in AGN disks can display unique features, owing to the unusual relative position of the shocks that characterize the burst evolution and the Thomson photosphere of the AGN disk. In dense environments, for example, a relativistic reverse shock develops early, likely powering the prompt emission instead of internal shocks. The transient's time evolution is also compressed, yielding afterglow emission that is brighter and may peak earlier than for GRBs in the interstellar medium. Additionally, in regions of the disk that are sufficiently dense and extended, the light curves are dominated by diffusion, since the fireball remains inside the disk photosphere throughout the entire evolution. These diffusion-dominated transients emerge on timescales of days in disks around SMBHs of $\sim 10^6 M_\odot$ to years for SMBHs of $\sim 10^8 M_\odot$. Finally, a large fraction of events, especially in AGNs with SMBHs $\lesssim 10^7 M_\odot$, display time-variable absorption in the X-ray band.

Unified Astronomy Thesaurus concepts: Active galactic nuclei (16); Gamma-ray bursts (629); Relativistic jets (1390)

1. Introduction

The accretion disks of active galactic nuclei (AGNs) have had a long history of study, as they are the engines powering the observed emission (Lynden-Bell 1969). Since the pioneering work on the disk structure by Shakura & Sunyaev (1973), increasingly more sophisticated models have been developed to understand the detailed structure of the disk (e.g., Sirko & Goodman 2003; Thompson et al. 2005), as well as to characterize the various regions surrounding the disk, and hence understand the physical reasons for the observational diversity of these sources.

In the last few years, the interest in AGN disks has expanded from their being sources of power for the supermassive black holes (SMBHs) at their centers, to their being hosts to stars and hence the compact objects that they leave behind. Broadly speaking, stars can end up in the disks of AGNs via two mechanisms: in situ formation resulting from disks becoming self-gravitating and unstable to fragmentation (e.g., Paczynski 1978; Goodman 2003; Dittmann & Miller 2020), and capture from the nuclear star cluster surrounding the AGN (e.g., Artymowicz et al. 1993; Fabj et al. 2020), as a result of momentum and energy loss as the stars interact with the disk.

Massive stars leave behind neutron stars and black holes, which then interact with the dense environment of the disk, resulting in migration within the disk, and enhanced probability of mergers (e.g., Bellovary et al. 2016; Secunda et al. 2019; Tagawa et al. 2020). The presence of compact objects, and their mergers, in AGN disks has become especially relevant in light of recent LIGO results: the detection of a binary BH merger with one of the BHs with mass above the pair instability range (Abbott et al. 2020), and another merger with at least one of the two compact objects in the lower mass gap (Abbott et al. 2020).

Both can be explained in an AGN disk scenario via a combination of hierarchical mergers and accretion of compact objects initially formed via standard evolutionary channels (e.g., McKernan et al. 2012; Bartos et al. 2017; Stone et al. 2017; McKernan et al. 2018; Yang et al. 2019; Tagawa et al. 2020).

In an AGN environment even binary BH mergers may be accompanied by an electromagnetic signature (McKernan et al. 2019). Here we focus on the presence of massive stars in AGN disks. A fraction of these, whose inner regions are endowed with sufficient angular momentum to form an accretion disk around the BH formed from the core upon collapse, is expected to also give rise to long GRBs (e.g., MacFadyen & Woosley 1999; Woosley & Heger 2006; Yoon et al. 2006), in addition to a supernova (Woosley & Bloom 2006). Long GRBs are predicted to occur mostly in low-metallicity environments (Woosley & Heger 2006; Yoon et al. 2006), where stellar cores are more likely to spin rapidly at core collapse due to reduced stellar mass loss. This is supported by observations of the bulk population (e.g., Graham & Fruchter 2013), although some long GRBs may also occur at solar or even super-solar metallicities (Levesque et al. 2010). While the metallicity of AGN disks tends to be high at all redshifts (e.g., Maiolino & Mannucci 2019), the evolution of stars in AGN disks might be substantially different from that in standard galactic environments (Cantiello et al. 2020), possibly resulting in a high fraction of rapidly rotating massive stars (A. Jermyn et al. 2020, in preparation). Additionally, as AGN disks favor mergers, NS–NS and NS–BH mergers are also expected. Both of these are believed to be progenitors of short GRBs (Berger 2014), which has been confirmed for the case of an

NS–NS merger (Abbott et al. 2017a, 2017b; Lazzati et al. 2018).

With both long and short GRBs expected to occur in AGN disks, the question of their observability arises. Can the relativistic jets associated with these astrophysical transients emerge from the dense environment of the AGN disk? Can their luminosity outshine the AGN copious emission at some wavelengths? And, if so, do their light curves present peculiar features that make them distinguishable from the rich range of AGN variability, as well as from GRBs occurring in more typical galactic environments?

Here we perform the first investigation of the properties of a relativistic jet evolving in the dense environment of an AGN disk. We focus our analysis on the relevant radii that determine the main features of the observable radiation. These radii are discussed in Section 2, and their magnitude is computed for two models of AGN disks in Section 3, together with the relevant timescales and transient luminosity. We summarize our results and their implications in Section 4.

2. GRBs in AGN Disks: Relevant Radii and Phenomenology

The following discussion relies on the standard internal/external shock model for the production of the γ-ray prompt radiation and the following afterglow emission (e.g., Piran 1999). Within this scenario, the highly variable γ-ray radiation is produced via the collisions of multiple relativistic shells produced by the newly formed BH from the star's core collapse. The collision timescale between two shells is reflected in the timescale between two pulses of γ-rays. Once the bulk of the shocks have collided, the relativistic outflow begins to be decelerated by the external medium that is collecting and an external shock is formed in the ambient material, giving rise to the longer wavelength afterglow radiation.

Within this model, which is schematically represented in Figure 1, there are six important radii that determine the evolution of the outflow/fireball and its observability. These are:

1. The *photospheric radius*, i.e., the radius at which the fireball becomes transparent. This is given by Daigne & Mochkovitch (2002) and Lazzati et al. (2020)

$$R_{\rm ph} = \frac{\sqrt{\left(\frac{cT_{\rm eng}}{1-\beta}\right)^2 + \frac{3}{2\pi}\frac{L_{\rm iso}Y_e\sigma_T T_{\rm eng}}{m_p c^2 \Gamma_\infty}} - \frac{cT_{\rm eng}}{1-\beta}}{2}, \quad (1)$$

where β is the outflow speed in units of the speed of light, Γ_∞ the asymptotic Lorentz factor, $T_{\rm eng}$ is the burst engine duration, σ_T the Thomson cross section, m_p the proton mass, Y_e the electron fraction in the outflow, and $L_{\rm iso} = E_{\rm iso}/T_{\rm eng}$ its isotropic luminosity, parameterized in terms of the isotropic outflow energy $E_{\rm iso}$.

2. The *internal shock radius*, i.e., the radius at which some of the bulk energy of the outflow is dissipated by collisions between shells that were ejected with different Lorentz factor. The bulk energy is transformed into internal energy that can be radiated. In the internal shock model, this is given by (e.g., Rees & Meszaros 1994; Piran 1999)

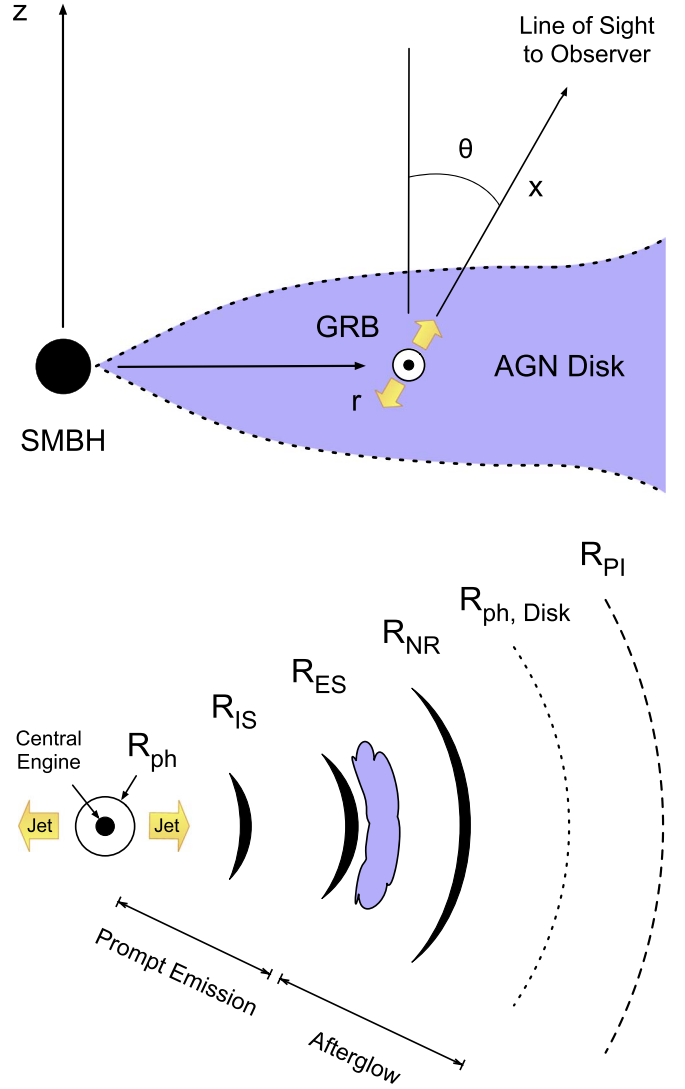$$R_{\rm IS} = c\Delta t \Gamma_\infty^2, \quad (2)$$

Figure 1. Schematic representation of the AGN disk geometry and our coordinate system (top) and the relevant radii in commonly observed GRBs in low density environments (bottom).

where Δt is the typical timescale between the emission of two shells, usually of the order of a fraction of a second.

3. The *external shock radius*, i.e., the radius at which the fireball dissipates its energy and an afterglow is formed (Mészáros & Rees 1997). The location of this radius depends on the thickness $\Delta = cT_{\rm eng}$ of the outflow shell and on its Lorentz factor (Sari & Piran 1995, 1999). More specifically,

$$R_{\rm ES} = \max[R_{\rm ES}^{\rm thin}, R_{\rm ES}^{\rm thick}]. \quad (3)$$

For a thin shell,

$$R_{\rm ES}^{\rm thin} = \left(\frac{3M_{\rm fb}}{4\pi\rho\Gamma_\infty}\right)^{1/3}, \quad (4)$$

where ρ is the density of the surrounding medium and $M_{\rm fb} = E_{\rm iso}/(c^2\Gamma_\infty)$ the fireball rest mass. This states that the external shock is formed when a shocked mass equal to the fireball rest mass reduced by a factor Γ_∞ has been

collected. For a thick shell,

$$R_{\mathrm{ES}}^{\mathrm{thick}} = \left(\frac{3E_{\mathrm{iso}}}{4\pi\rho c^2}\right)^{1/4} (cT_{\mathrm{eng}})^{1/4}, \qquad (5)$$

where T_{eng} is the duration of the GRB. This condition ensures that an external shock is formed only after the reverse shock has fully crossed the fireball.

4. The *nonrelativistic radius*, i.e., the radius at which the mass swiped up is large enough to cause the deceleration of the blast wave to nonrelativistic speed. This radius is also known as the Sedov length and is given by (e.g., Piran 1999):

$$R_{\mathrm{NR}} = \left(\frac{3E_{\mathrm{iso}}}{4\pi\rho c^2}\right)^{1/3}. \qquad (6)$$

5. The *disk photospheric radius* $R_{\mathrm{ph,Disk}}$, defined as the location within the disk from which the radiation can escape since the photons' mean free path for Thomson scattering becomes infinite. This is determined by solving the equation

$$\tau = \int_{R_{\mathrm{ph,Disk}}}^{\infty} dx \; n_{\mathrm{d}}(x)\sigma_{\mathrm{T}} = 1, \qquad (7)$$

where the variable $x(r, z)$ indicates the coordinate along the line of sight to the observer, and $n_{\mathrm{d}}[x(r, z)]$ is the local number density in the disk.

6. The *photoionization radius*, i.e., the radius out to which the ionizing radiation from the burst is abundant enough to cause complete ionization of all the elements of significant astrophysical abundance (typically, up to iron). In a cold and dense environment, this is given by:

$$R_{\mathrm{PI}} = \left[\frac{3}{4\pi n} \int_{t_0}^{\infty} dt \int_{\nu_0}^{\infty} d\nu \frac{L(\nu, t)\sigma(\nu)}{h\nu}\right]^{1/3}. \qquad (8)$$

In the case of AGN disks, however, this should be considered as a lower limit, since at typical disk temperatures the gas is at least partly ionized.[5]

In the traditionally studied cases both long and short GRBs explode in interstellar medium environments, and the above list ranks the radii from the smallest to the largest. However, the ordering can change for a burst exploding in a dense and extended region, such as that of an AGN disk. The radii affected by the ambient density are the external shock radius, the nonrelativistic radius, the disk photospheric radius, and the photoionization radius. The internal shock radius and fireball photospheric radius are instead independent of the density, hence leaving the possibility that both of them, or the internal shock radius only (typically larger than the photospheric radius of the fireball) can be smaller than the external shock radius. Under these circumstances, the developing external shock would drive a relativistic reverse shock into the jet, likely generating magnetic fields strong enough to power emission in the gamma-ray band. Note that this reverse-shock gamma-ray emission would be present irrespective of the existence of internal shocks, which are not universally accepted.[6] In the following, we assume that the radius R_{prompt} at which the

prompt emission is generated is the smallest between R_{IS} and R_{ES}. This does not consider photospheric emission, but even if that was the case, our conclusions would be unaffected.

We can then distinguish the following situations:

1. $R_{\mathrm{ph,Disk}} < R_{\mathrm{prompt}} < R_{\mathrm{ES}} < R_{\mathrm{NR}}$.
   This is a rather "standard" GRB, though the emission may come on faster timescales due to the higher densities (more on this in Section 3). The peak of the optical and X-ray afterglow emission happens at the time at which the external shock develops.

2. $R_{\mathrm{prompt}} < R_{\mathrm{ph,Disk}} < R_{\mathrm{ES}} < R_{\mathrm{NR}}$.
   In this case the prompt radiation occurs inside the disk photosphere, and hence it becomes isotropized and diluted in time via Thomson scattering. These effects result in a reduction of the intensity by a factor of $4\pi/\Omega_{\mathrm{j}}$, where Ω_{j} is the angular size of the jet, and by an additional factor $t_{\mathrm{diff}}/T_{\mathrm{eng}}$, where t_{diff} is the diffusion timescale. This timescale depends on the position of the radiating source within the disk, which changes with time for a relativistic fireball. In order to keep the discussion concise, we here assume that the transients are diffused as if they were in the plane of the disk, a worst-case scenario. In this case, the diffusion timescale is given by:

$$t_{\mathrm{diff}} \approx \frac{H^2\rho_0\sigma_T}{m_p c}, \qquad (9)$$

where H is the scale height of the disk and ρ_0 is the density in the disk midplane. In this case the external shock develops outside of the disk photosphere, and therefore the afterglow would appear typical, though on faster timescales. As in the previous case, the luminosity peak is determined by the timescale t_{ES} at which the external shock is formed.

3. $R_{\mathrm{prompt}} < R_{\mathrm{ES}} < R_{\mathrm{ph,Disk}} < R_{\mathrm{NR}}$.
   In this case the prompt emission is diluted and scattered as in the previous case, and so too is the early afterglow radiation. This dilution occurs until $t_{\mathrm{ES,d}}$, at which time the external shocks exit the disk photosphere and the afterglow emission peaks. From that time on, the afterglow emission proceeds as typical, though on faster timescales.

4. $R_{\mathrm{prompt}} < R_{\mathrm{ES}} < R_{\mathrm{NR}} < R_{\mathrm{ph,Disk}}$.
   In this case both the prompt emission and afterglow emission are isotropized, time-diluted, and thermalized by Thomson scattering, both arriving to the observer on the diffusion timescale discussed above (see Equation (9)).

3. Radii in Specific Models of AGN Disks and Observability of the Transients

In order to assess the conditions that can be verified in AGN disks, and hence the observational features that GRBs born out of AGNs would have, we consider two specific models of AGN disks: the one by Sirko & Goodman (2003; SG in the following) and the one by Thompson et al. (2005; TQM in the following). The density profile in the disk is described by an isothermal atmosphere model,

$$\rho_{\mathrm{disk}}(r, z) = \rho_0(r)\exp\left[-\frac{z^2}{2H^2(r)}\right], \qquad (10)$$

---

[5] Also note that, even in regions that may be dominated by dust, this is very effectively destroyed by the early UV/X-ray radiation from the burst.

[6] In this case, the prompt emission would be released at the photosphere (e.g., Lazzati et al. 2009), which would be unmodified even in a disk environment.
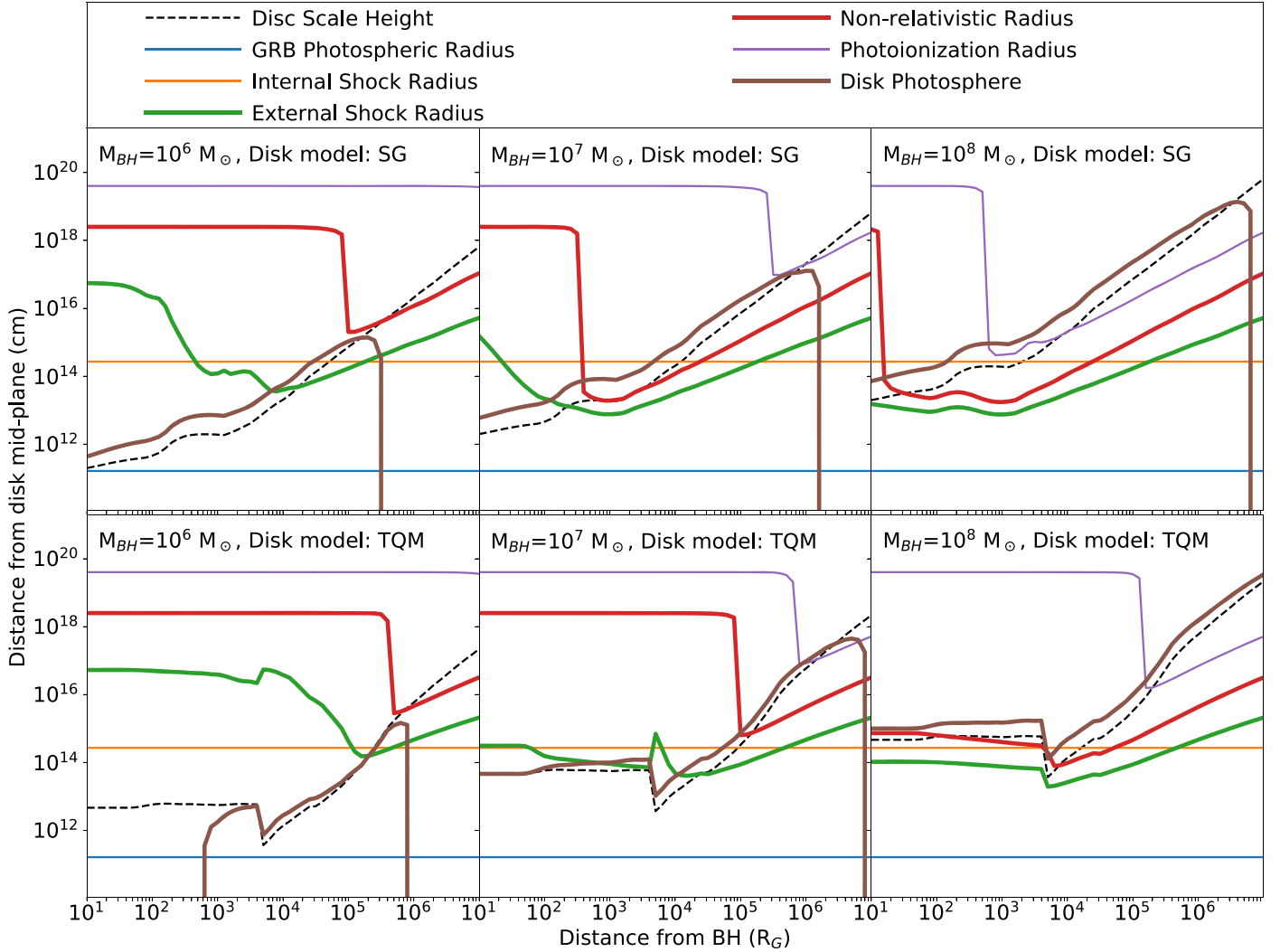
Figure 2. The relevant radii for relativistic jets generated in AGN disks, for three values of the SMBH mass. The jet source is assumed to be located in the midplane of the disk, and the line of sight to the observer is perpendicular to the disk plane. The density profile of the disk is adopted from the model of Sirko & Goodman (2003) in the top panels and from Thompson et al. (2005) in the bottom ones. The disk scale height for each model is indicated with the black dashed line.

with the profiles $\rho_0(r)$ (the density in the disk midplane) and $H(r)$ (the disk scale height) provided by the AGN models referenced above (see Figure 1 in Fabj et al. 2020 for a visual comparison between the main properties of these disks).

The relevant radii introduced in Section 2 are computed[7] and displayed in Figure 2 for the SG (top panels) and TQM (bottom panels) disk structures. In each case, we consider three values for the mass of the central SMBH: 10^6, 10^7, and $10^8 M_\odot$, which encompass a large fraction of measured masses of SMBHs in AGNs.[8] The black dashed line guides the eye to the location of the scale height of the disk, as compared to the relevant source-related radii. The location of the source is assumed to be at the disk midplane, while the line of sight to the observer is perpendicular to the disk plane.

For the computation of GRB-specific radii, we use generic parameter values as typical for long GRBs (e.g., Ghirlanda et al. 2018): $E_{\rm iso} = L_{\rm iso}T_{\rm eng} = 10^{53}$ erg, with $T_{\rm eng} = 20$ s, $Y_e = 1$, $\eta = 300$, and $\Delta t = 0.1$ s. In all the circumstances considered, the photospheric radius is the smallest among all the radii. Note that this would be even more so the case for a short GRB (smaller $E_{\rm iso}$) and shorter $T_{\rm eng}$; hence the following considerations can be considered generally holding for both long and short GRBs.

Let us start by examining the $M = 10^6 M_\odot$ cases: in both disk models the fireball exits the disk photosphere while still relativistic, and hence there will always be some standard afterglow radiation. At small and large disk radii ($\lesssim 10^4$ or $\gtrsim 3 \times 10^6 R_G$ in the SG model and $\lesssim 10^5$ or $\gtrsim 10^6 R_G$ in the TQM model, where R_G is the gravitational radius), the internal and external shock radii are also outside the disk photosphere, and the full prompt and afterglow will be observed. A strong, relativistic reverse shock is expected in most cases, since these outflows are characterized by thick shells (Sari & Piran 1995, 1999). The photoionization radius (computed for a typical GRB Band spectrum, Band et al. 1993), is well outside the disk photosphere. This implies that the early UV/
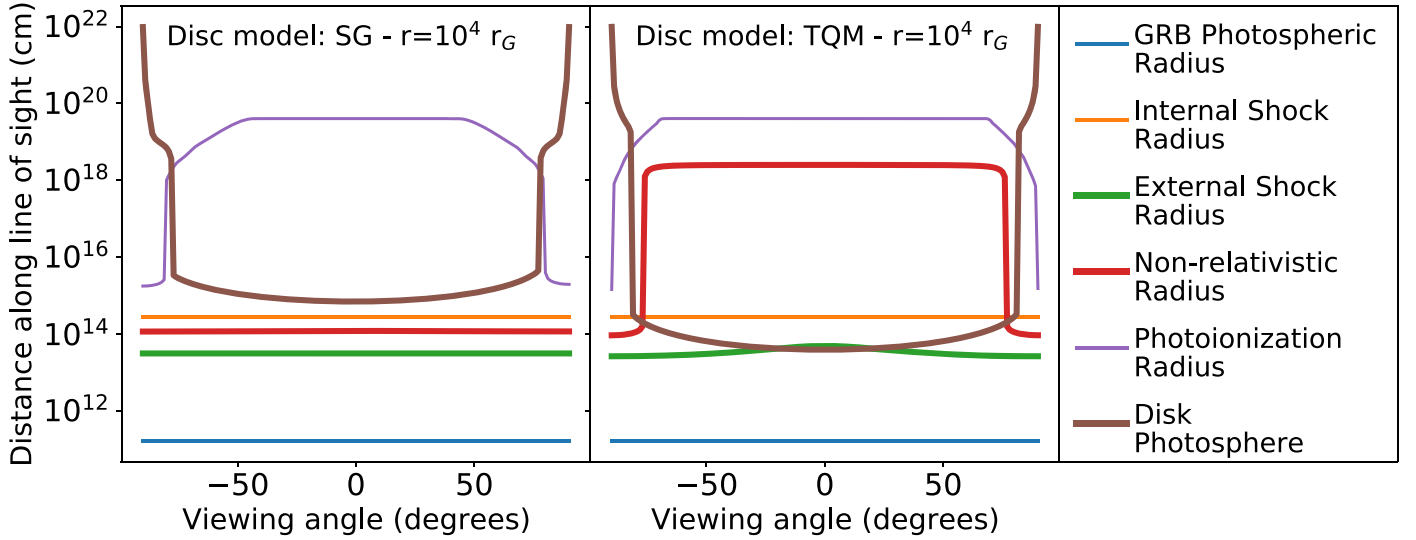
---

[7] We use the standard expressions for fireball evolution in the ISM. However, note that a relativistic shock is known to accelerate in an exponential atmosphere (Perna & Vietri 2002) as well as in a density profile ρ^{-k} with $k > 4.13$ (Best & Sari 2000). In an AGN disk the atmosphere is exponential in the z direction, declining but shallower than $\rho^{-4.13}$ in the outward direction, and increasing inward. A detailed radius evolution can thus only be computed numerically.

[8] http://www.astro.gsu.edu/AGNmass/

Figure 3. Relevant radii as a function of the viewing angle for a representative case with SMBH mass of $10^7 M_\odot$ and a distance from the BH of $R = 10^4 R_G$.

X-ray flux photoionizes the medium along its line of sight, resulting in time-variable absorption, if measured with time-resolved X-ray spectroscopy (Lazzati & Perna 2002; Perna & Lazzati 2002).

As the SMBH mass increases to $10^7 M_\odot$, GRBs in the outer parts of the disk ($\gtrsim 10^2 R_G$ for the SG model and $\gtrsim 10^5 R_G$ for the TQM disk) become nonrelativistic inside the disk photosphere, and hence in those regions only longer-lived, diffusion-dominated transients will be observed. At small radii ($\lesssim 10^2 R_G$ in both disk models) the external model develops outside the disk photosphere and both prompt and afterglow emission are unobscured. In both models, however, there are intermediate radii where both the prompt emission and the early afterglow are diluted on $t_{\rm diff}$, while the later afterglow develops normally. Photoionization of the medium by the GRB is also expected up to large disk radii, $\sim 10^5 R_G$.

For the case with even larger SMBH mass, $10^8 M_\odot$, the general expectation, irrespective of the disk model, is that of a dim and long transient, diluted on the timescale $t_{\rm diff}$. Note that, while Figure 2 is calculated for a line of sight perpendicular to the disk, the outcome is similar for a large range of viewing angles θ, as shown in Figure 3.

To further quantify the observable properties of the transients, we compute the timescales corresponding to the relevant radii discussed above. These are displayed in Figure 4. In a standard afterglow, the timescale of the peak emission at optical frequencies and above is given by that of formation of the external shock, $t_{\rm ES}$. However, if the early afterglow is produced inside the disk photosphere, the peak emission occurs at the time $t_{\rm ES,Disk}$, at which the fireball crosses the disk photosphere. Hence, more generally, the time of the peak emission is the largest between $t_{\rm ES}$ (green line in Figure 4) and $t_{\rm ES,Disk}$ (brown line in the same figure). Peak times are longer when the shock becomes nonrelativistic inside the disk photosphere, in which case the transient emerges on the timescale $t_{\rm diff}$, indicated with a purple line in Figure 4. The light curve peaks at the longest of the three mentioned times, as indicated with the dashed pink line. Note that in the thick shell case the afterglow peaks approximately at the end of the prompt emission.

We summarize these results and extend them to a continuum of SMBH masses in Figure 5. Blue areas indicate typical

GRBs, for which both the prompt γ-rays and the later afterglow radiation are produced after the fireball has exited the disk photosphere. Salmon regions are diffusion-dominated for the prompt γ-ray transient and early afterglow, but display a normal afterglow later, when the external shock crosses the disk photosphere. In these regions the black contours indicate the peak times of the afterglow: $t_{\rm ES}$ in the green regions and $t_{\rm ES,Disk}$ in the salmon regions. Green areas are the ones in which both the γ-ray transient and the afterglow are produced inside the disk photosphere, and hence emerge diluted on the diffusion timescale. The black contours in these regions indicate the diffusion time.[9]

The extremely high densities of the medium in an AGN disk, while shortening the timescale of the emission, also make it brighter. For an adiabatic fireball, the peak afterglow luminosity is given by Sari et al. (1998)

$$L_{\nu,\rm peak} = 4.4 \times 10^{39} \epsilon_{B,-1}^{1/2} E_{53} n_{12}^{1/2} \, {\rm erg \, s^{-1} \, Hz^{-1}}, \quad (11)$$

where $E_{53} = E_{\rm iso}/10^{53}$ erg, $n_{12} = n/10^{12}$ cm^{-3}, and $\epsilon_{B,-1} = \epsilon_B/0.1$ is the fraction of shock energy that goes into magnetic energy. At an optical frequency of $\nu_O = 5 \times 10^{14}$ Hz, the peak luminosity becomes $L_{\rm peak} = \nu_O L_{\nu_O,\rm peak} \sim 2 \times 10^{54} E_{53} n_{12}^{1/2}$ erg s^{-1}. This maximum luminosity is reached in the case in which the reverse shock is produced outside of the disk photosphere (with magnitude clearly dependent on the local medium density). In the case in which it is produced inside, the peak luminosity depends on the time at which it exits the photosphere, which in turns depends on the specific location within the disk.

To generalize the discussion of the transient luminosity while keeping it simple, we can alternatively estimate the bolometric afterglow luminosity using the observation that a fraction $\eta_{\rm aft}$ of the total fireball energy is dissipated in the afterglow. The peak luminosity can then be simply estimated as $L_{\rm peak,bol} \sim \eta_{\rm aft} E/t_{\rm peak} = 10^{53} E_{53} \eta_{\rm aft}/(t_{\rm peak} \, {\rm s}^{-1})$ erg s^{-1}. The brightness contrast with the AGN disk luminosity will depend on the observation band. Most AGNs have bolometric luminosities $\sim 10^{43-47}$ erg s^{-1} spread across the spectrum but

---

[9] Our results are broadly consistent with those of Zhu et al. (2020), which appeared while our paper was under review.
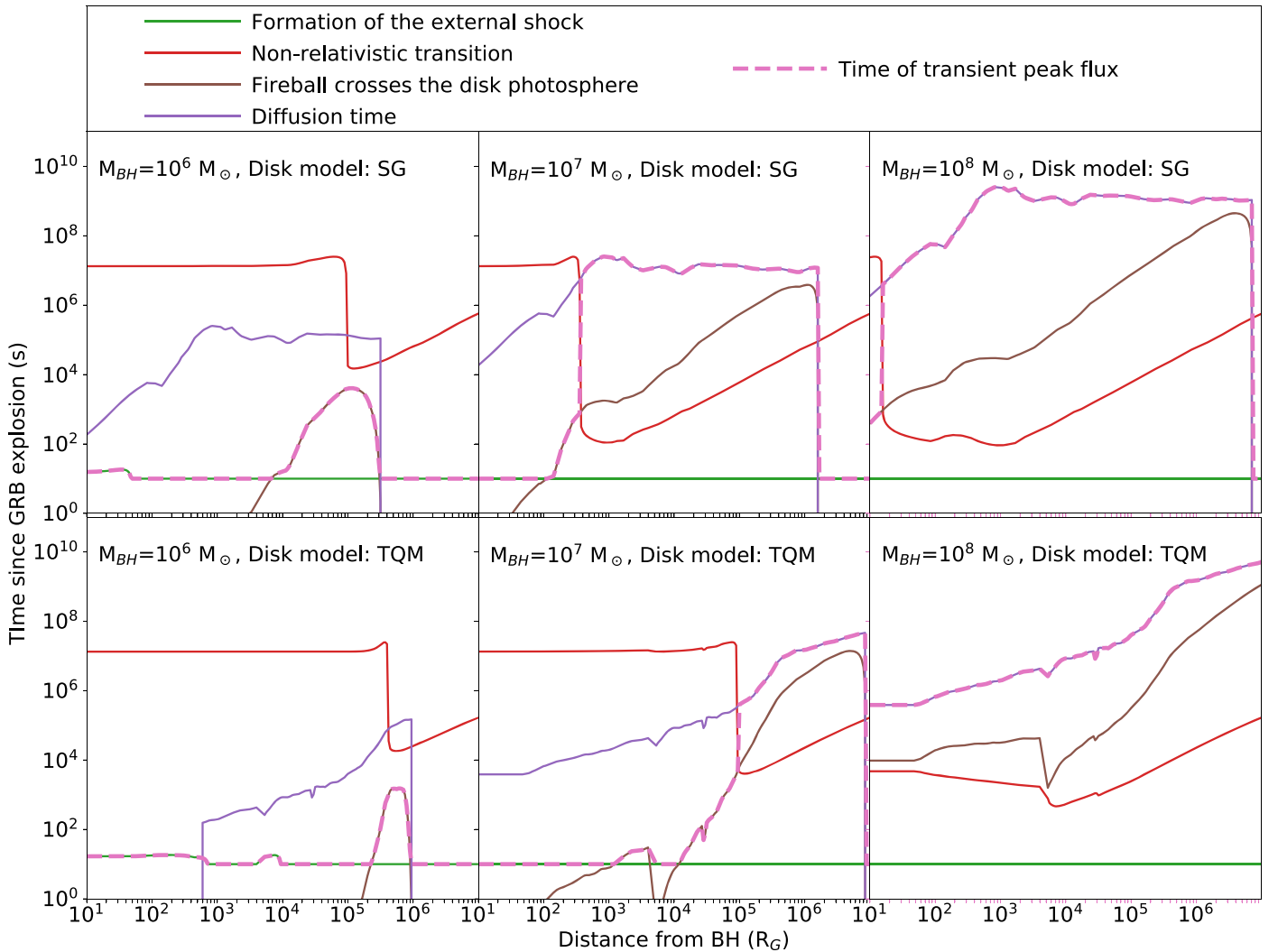
Figure 4. Timescales of the afterglow transient. The observed time for the external shock formation, transition to nonrelativistic expansion, and crossing of the photosphere are plotted along with the diffusion timescale for a source in the disk midplane. A thicker dashed line is used to show the expected time of maximum observed flux of the afterglow transient. The density profile of the disk is adopted from the model of Sirko & Goodman (2003) in the top panels and from Thompson et al. (2005) in the bottom ones, as in Figure 2.

with a large fraction in the UV/optical (e.g., Woo & Urry 2002). If a fraction f_O of the afterglow luminosity is emitted in the optical band, then transients with $t_{\rm peak} \lesssim 2 \times 10^5$ s ($\sim$2 days) will be $\sim$5 times brighter than an AGN with an average optical luminosity of $\sim 10^{45}$ erg s^{-1}. Here we have assumed $\eta_{\rm aff} f_O = 10^{-2}$, an estimate that yields Equation (11) for a nondiffused transient. Note, however, that for diffusion-dominated transients the peak luminosity decreases by a factor of $4\pi/\Omega_j \sim 100$ due to the isotropization of the beamed afterglow photons. In other bands, such as X-rays, IR, and radio, the transient will generally be easily detectable against the background AGN. Multiwavelength monitoring will be key to distinguish diffusion-dominated GRB afterglows from other transients, since their energetics and timescales would be similar to those of core-collapse supernovae, but their spectra are expected to remain much wider in frequency. Multimessenger signals, such as gravitational waves and/or neutrinos, could also be insightful for nearby events.

Last, in order to put our calculations in a broader context, we make an estimate of the rate of different types of stellar explosions in AGNs. We note that massive stars in AGN disks can originate from in situ formation, or be captured from nearby nuclear stellar clusters. While it is hard to predict the number of massive stars that can form during a typical AGN phase ($\sim 10^7$ yr), stellar capture and subsequent rapid accretion should yield about 10^2–10^4 massive stars in the disk (Cantiello et al. 2020). Given an AGN number density of 2×10^4 Gpc^{-3} (e.g., Greene & Ho 2007) this results in a core-collapse supernova rate of [0.2, 20] Gpc^{-3} yr^{-1}. The fraction that could also produce a long GRB depends on the final angular momentum distribution of the accreting massive star's progenitors (A. Jermyn et al. 2020, in preparation). These explosive outcomes are expected to occur preferentially in the inner regions of AGNs, where the rate of capture and the Bondi–Hoyle–Littleton accretion rate are higher. This has implications for the typical local AGN conditions surrounding these events and their EM signatures (see Figure 5). Concerning short GRBs, McKernan et al. (2020) claim that the rates of BH–NS and NS–NS mergers are $f_{\rm agn} \times$ [10, 300] Gpc^{-3} yr^{-1} and $\leqslant f_{\rm agn} \times 400$ Gpc^{-3} yr^{-1}, respectively, where $f_{\rm agn}$ is the currently unknown fraction of events detected by LIGO/Virgo coming from an AGN channel.
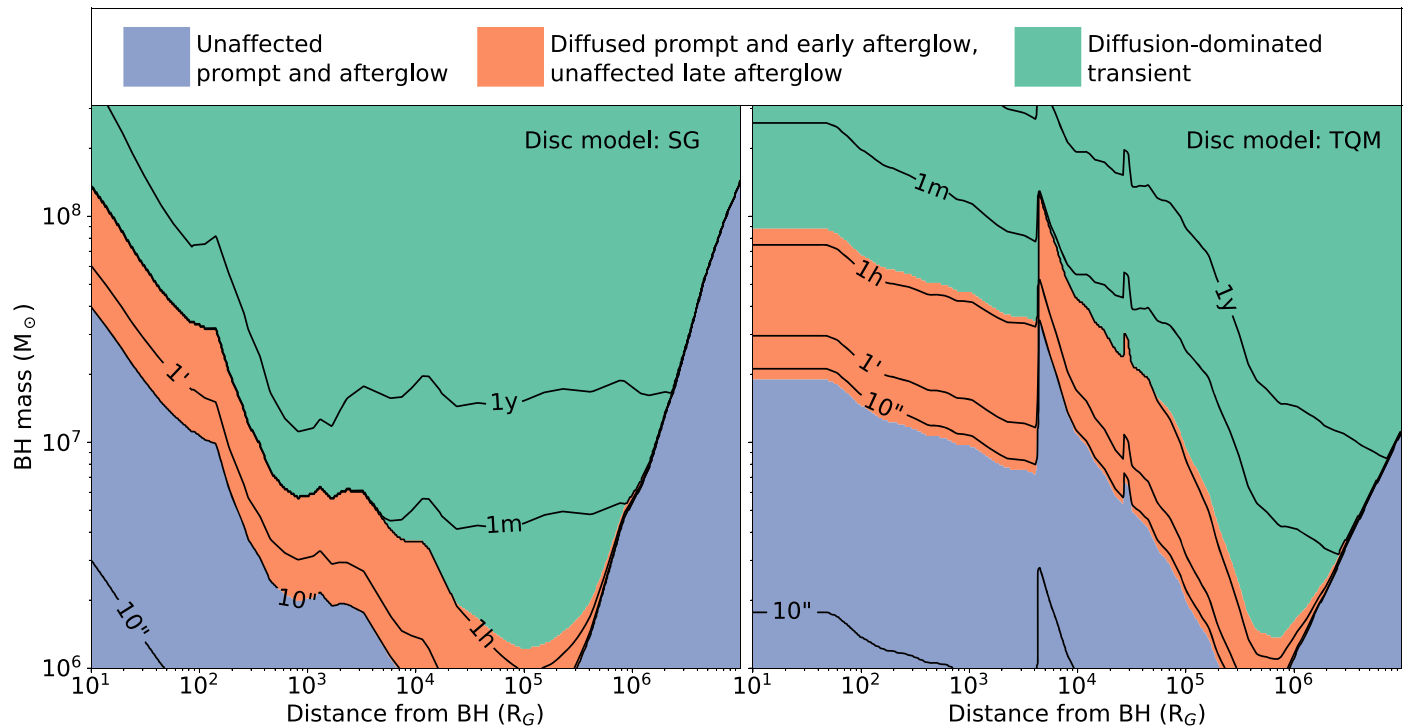
Figure 5. Schematic view of the various possibilities for the outcome of a GRB from an AGN disk. Blue regions: normal GRBs. Salmon: diffusion-dominated prompt γ-rays and early afterglows but normal late afterglow. Green: both prompt radiation and afterglow emerge on a diffusion timescale. The black lines indicate the time at which the electromagnetic transient peaks.

4. Summary

AGN disks are emerging as rich environments for hosting stars and the NSs and BHs that the most massive ones leave behind upon their deaths. Formation of binary compact objects and mergers are enhanced in disk environments. Both long and short GRBs are hence expected to occur in AGN disks, the former from a fraction of massive and quickly rotating stars, the latter from NS–NS to possibly NS–BH mergers.

Both types of transients are produced by relativistic fireballs, and here we have addressed the timely question of their evolution in the special environments of AGN disks, and the observability of the prompt and afterglow radiation that they produce. Our analysis has uncovered some unique features, especially evident in the lower mass SMBHs, in which cases the fireball emerges from the disk photosphere while still relativistic. In particular, due to the very high densities of AGN disks, the external shock generally forms before the internal shocks, hence potentially yielding a strong reverse shock. Under these conditions, while no γ-rays would be formed in internal shocks, they may be produced by the powerful reverse shock.

The time at which the afterglow emission peaks is determined, for a large fraction of disk radii and as long as the fireball remains relativistic up to the disk photosphere, by the time it takes for the fireball to cross the disk photosphere, rather than by the typical timescale for the external shock to form. On the other hand, in disk regions in which the fireball becomes nonrelativistic prior to exiting the disk photosphere, the radiation will emerge on the diffusion timescale, which varies from between a few days to a few years for AGN disks around SMBHs of masses in the $10^6 - 10^8 M_\odot$ range. Last, for transients with early monitoring of the X-ray emission, time-variable absorption is generally expected. Future works will be devoted to further explore and quantify via numerical simulations several aspects of this first analysis.

ORCID iDs

Rosalba Perna https://orcid.org/0000-0002-3635-5677
Davide Lazzati https://orcid.org/0000-0002-9190-662X
Matteo Cantiello https://orcid.org/0000-0002-8171-8596

References

Abbott, B. P., Abbott, R., Abbott, T. D., et al. 2017a, PhRvL, 119, 161101
Abbott, B. P., Abbott, R., Abbott, T. D., et al. 2017b, ApJL, 848, L12
Abbott, B. P., Abbott, R., Abbott, T. D., et al. 2020, ApJL, 892, L3
Abbott, R., Abbott, T. D., Abraham, S., et al. 2020, PhRvL, 125, 101102
Artymowicz, P., Lin, D. N. C., & Wampler, E. J. 1993, ApJ, 409, 592
Band, D., Matteson, J., Ford, L., et al. 1993, ApJ, 413, 281
Bartos, I., Kocsis, B., Haiman, Z., & Márka, S. 2017, ApJ, 835, 165
Bellovary, J. M., Mac Low, M.-M., McKernan, B., & Ford, K. E. S. 2016, ApJL, 819, L17
Berger, E. 2014, ARA&A, 52, 43
Best, P., & Sari, R. 2000, PhFl, 12, 3029
Cantiello, M., Jermyn, A. S., & Lin, D. N. C. 2020, arXiv:2009.03936
Daigne, F., & Mochkovitch, R. 2002, MNRAS, 336, 1271
Dittmann, A. J., & Miller, M. C. 2020, MNRAS, 493, 3732
Fabj, G., Nasim, S. S., Caban, F., et al. 2020, MNRAS, 499, 2608

Ghirlanda, G., Nappo, F., Ghisellini, G., et al. 2018, A&A, 609, A112
Goodman, J. 2003, MNRAS, 339, 937
Graham, J. F., & Fruchter, A. S. 2013, ApJ, 774, 119
Greene, J. E., & Ho, L. C. 2007, ApJ, 667, 131
Lazzati, D., Ciolfi, R., & Perna, R. 2020, ApJ, 898, 59
Lazzati, D., Morsony, B. J., & Begelman, M. C. 2009, ApJL, 700, L47
Lazzati, D., & Perna, R. 2002, MNRAS, 330, 383
Lazzati, D., Perna, R., Morsony, B. J., et al. 2018, PhRvL, 120, 241103
Levesque, E. M., Kewley, L. J., Berger, E., & Zahid, H. J. 2010, AJ, 140, 1557
Lynden-Bell, D. 1969, Natur, 223, 690
MacFadyen, A. I., & Woosley, S. E. 1999, ApJ, 524, 262
Maiolino, R., & Mannucci, F. 2019, A&ARv, 27, 3
McKernan, B., Ford, K. E. S., Bartos, I., et al. 2019, ApJL, 884, L50
McKernan, B., Ford, K. E. S., Bellovary, J., et al. 2018, ApJ, 866, 66
McKernan, B., Ford, K. E. S., Lyra, W., & Perets, H. B. 2012, MNRAS, 425, 460
McKernan, B., Ford, K. E. S., O'Shaughnessy, R., & Wysocki, D. 2020, MNRAS, 494, 1203
Mészáros, P., & Rees, M. J. 1997, ApJ, 476, 232

Paczynski, B. 1978, AcA, 28, 91
Perna, R., & Lazzati, D. 2002, ApJ, 580, 261
Perna, R., & Vietri, M. 2002, ApJL, 569, L47
Piran, T. 1999, PhR, 314, 575
Rees, M. J., & Meszaros, P. 1994, ApJL, 430, L93
Sari, R., & Piran, T. 1995, ApJL, 455, L143
Sari, R., & Piran, T. 1999, ApJ, 520, 641
Sari, R., Piran, T., & Narayan, R. 1998, ApJL, 497, L17
Secunda, A., Bellovary, J., Mac Low, M.-M., et al. 2019, ApJ, 878, 85
Shakura, N. I., & Sunyaev, R. A. 1973, A&A, 500, 33
Sirko, E., & Goodman, J. 2003, MNRAS, 341, 501
Stone, N. C., Metzger, B. D., & Haiman, Z. 2017, MNRAS, 464, 946
Tagawa, H., Haiman, Z., & Kocsis, B. 2020, ApJ, 898, 25
Thompson, T. A., Quataert, E., & Murray, N. 2005, ApJ, 630, 167
Woo, J.-H., & Urry, C. M. 2002, ApJ, 579, 530
Woosley, S. E., & Bloom, J. S. 2006, ARA&A, 44, 507
Woosley, S. E., & Heger, A. 2006, ApJ, 637, 914
Yang, Y., Bartos, I., Gayathri, V., et al. 2019, PhRvL, 123, 181101
Yoon, S. C., Langer, N., & Norman, C. 2006, A&A, 460, 199
Zhu, J.-P., Zhang, B., Yu, Y.-W., & Gao, H. 2020, arXiv:2011.08428